ChemComm

Accepted Manuscript

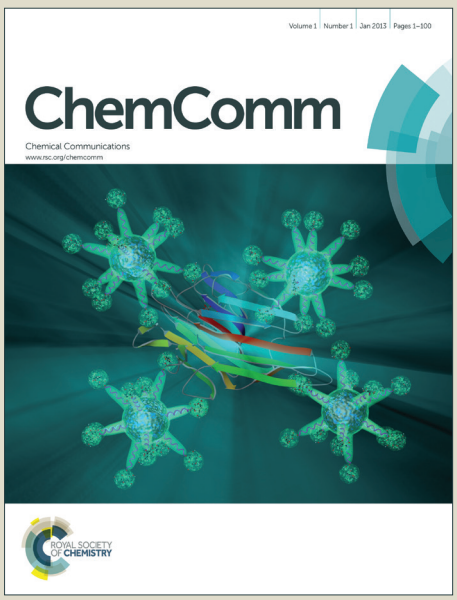

ROYAL SOCIETY OF CHEMISTRY

www.rsc.org/chemcomm

Journal Name

RSCPublishing

COMMUNICATION

A hybrid gel/solid-state polymer electrolyte for long-life lithium oxygen batteries

Cite this: DOI: 10.1039/xoxxoooooox

Received ooth January 2012,
Accepted ooth January 2012

DOI: 10.1039/xoxxoooooox

www.rsc.org/

Wen-Bin Luo[a], Shu-Lei Chou[a]*, Jia-Zhao Wang[a], Yong-Mook Kang[b]*, Yu-Chun Zhai[c], Hua-Kun Liu[a]

A hybrid gel/solid-state polymer electrolyte has been used as the separator and electrolyte for the lithium oxygen battery. It can not only avoid electrolyte evaporation but also protect the lithium metal anode during reactions over long-term cycling. Due to its high ionic conductivity and low activation energy, excellent cycling performance is demonstrated, in which the terminal voltage is higher than 2.2 V after 140 cycles at 0.4 mA cm^{-2}, with 1000 mAh g^{-1}$_{(composite)}$ capacity.

The non-aqueous lithium oxygen battery is a promising candidate for the next-generation energy storage system because of its potentially high energy density (up to 2-3 kW kg^{-1}), exceeding that of any other existing energy storage system for storing sustainable and clean energy to reduce greenhouse gas emissions and the consumption of non-renewable fossil fuels. It stores and converts energy between chemical energy and electrical energy via a reversible reaction of lithium and oxygen ($2Li^+ + O_2 + 2e^- = Li_2O_2$).[1-4] At present, the non-aqueous lithium oxygen battery is typically composed of a lithium metal anode, a porous air cathode open to O_2 in the atmosphere, and a lithium-ion-conducting organic liquid electrolyte between the two electrodes.[5-7] According to recent published reports, this battery design has significant technical defects: (i) the liquid electrolyte evaporates or dries out during long-term cycling; (ii) the lithium metal anode directly reacts with oxygen; and (iii) liquid electrolytes limit choices in cell design due to their fluidic characteristics and the need for separator membranes in the cell assembly.[3,8-13] Therefore, replacing the liquid electrolytes may be another promising strategy to address the challenges mentioned above, by such alternatives as gel-polymer electrolyte or solid-state electrolyte.[13-17] Gel-polymer electrolytes (GPEs) which are generally composed of liquid electrolyte in a polymer matrix, are widely used in lithium ion batteries owing to their excellent ionic conductivity, high safety, and mechanical flexibility.[18-22] Solid electrolytes are good to prevent the oxygen diffusion but with low ionic conductivity.[24-26] Therefore, it would be good to combine both solid electrolyte and gel-electrolyte together to form a hybrid electrolyte to achieve both high ionic conductivity and good protection for Li to directly contact and react with O_2. On the other hand, it is worth considering the deposition of Li_2O_2 during discharge: the oxygen reduction reaction (ORR, $O_2 + 2Li^+ + 2e^- \rightarrow Li_2O_2$), and the decomposition of Li_2O_2 during the charge process: the oxygen evolution reaction (OER, $Li_2O_2 \rightarrow O_2 + 2Li^+ + 2e^-$), which are two important processes that determine the performance of Li-O_2 cells.[5,7,9,12] To achieve high energy and long-term cycling stability, an efficient electrocatalyst plays an important role in the ORR and OER. Ruthenium based nanoparticles have already been actively employed as catalysts in various areas, such as the water splitting oxygen evolution reaction,[27-29] CO oxidation,[30,31] alcohol oxidation,[32,33] and amine oxidation.[34] Recently, Shao-Horn's and other groups confirmed the catalytic activity of RuO_2 towards oxygen evolution in acid and alkaline aqueous solutions, also showing that its stability under OER conditions is higher than that of ruthenium carbon composites.[7,27,35,36] In order to go on to make a high dispersion, low aggregation, and large surface area catalyst, two-dimensional nitrogen-doped graphene catalyst support has been used.[37] Therefore, in this work, we have designed a special flexible lithium oxygen battery device using gel-solid polymer electrolyte, which can not only avoid electrolyte evaporation, but also protects the lithium metal anode during reaction. RuO_x nanoparticles decorated uniformly on nitrogen-doped graphene were employed as the cathode material. This system exhibits excellent rechargeability performance

The general process for the system is illustrated in Figure 1. Typically, the composite, RuO_x decorated on the nitrogen doped reduced graphene oxide (N-rGO@RuO_x), is obtained by the microwave hydrothermal method. The first step is to coat the obtained N-rGO@RuO_x on the gas diffusion layer, following by brushing on a gel-polymer electrolyte (GPE) layer to a thickness of about 1-2 mm. Then, the above cathode electrode is exposed to an ultraviolet (UV) lamp for different times to drive the polymerization reaction to form a solid-state layer. For the anode electrode preparation, about 1-2 mm of GPE is brushed on one side of a piece of nickel foam, and the lithium metal is attached on the other side of the nickel foam. The schematic diagram in Fig. 1(h) shows the internal structure of the lithium oxygen battery device. The gel-solid layer and the nickel foam immersed in GPE were designed to avoid the electrolyte evaporation and protect the lithium metal anode from oxidization.

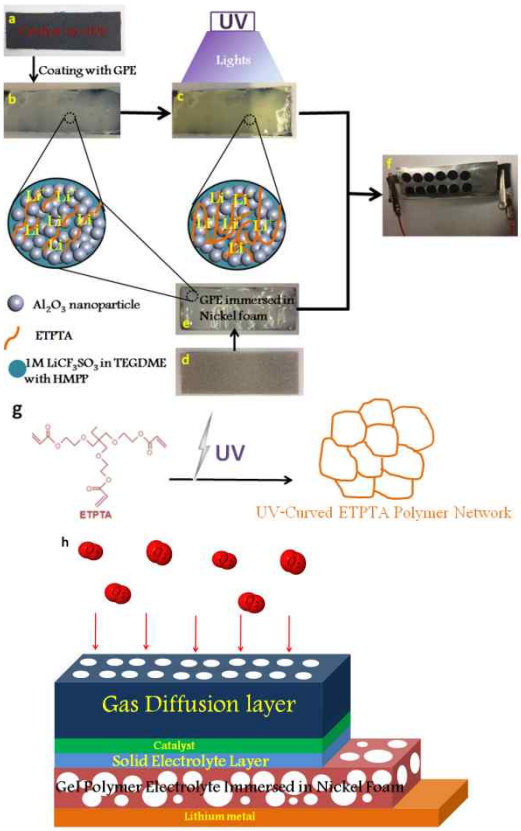

Figure 1. Schematic flow-process diagram of the fabrication of the flexible lithium oxygen battery system: (a) gas diffusion layer (GDL) coated with N-rGO@RuO_x; (b) gel-polymer electrolyte brushed on the side of GDL coated with N-rGO@RuO_x; (c) air electrode after polymerization to form a solid layer; (d) nickel foam; (e) fill the nickel foam with the obtained gel polymer electrolyte and brush about 1mm on the side of the nickel form;(f) photograph of flexible lithium oxygen battery; (g) the process of polymerization to form a polymer network; (h) schematic diagram of the internal structure of the device. TEGDME: tetraethylene glycol dimethyl ether; ETPTA: ethoxylated trimethylolpropane triacrylate; HMPP: 2-hydroxy-2-methyl-1-phenyl-1-propanon.

The as-prepared cathode materials were characterized by Raman spectroscopy and high-resolution transmission electron microscopy (HRTEM), as shown in Figures 2(a, b) and S1 in the Supporting Information (SI). Compared with pure rGO, thre are two corresponding Raman bands at 1590 cm^{-1} (G band) and 1325 cm^{-1} (D band), but two additional Raman bands also appear at the positions of ~ 510 and ~ 620 cm^{-1} for N-rGO@RuO_x composite, which correspond to the Ru-O bonding shift.[38] HRTEM analysis was employed to determine the morphology and the particle size distribution of the RuO_x nanoparticles on the rGO. The as-prepared rGO nanosheets have a laminar structured morphology, and the RuO_x nanoparticles are uniformly attached on the nanosheets. The size of most nanoparticles is in the range of 1–3 nm. The composite was also characterized by X-ray diffraction (XRD), as shown in Fig.S2, although there are no obvious RuO_x signals, which may have resulted from the small particle size.

X-ray photoelectron spectroscopy (XPS) was further used to gain insight into the chemical bonding in N-rGO@RuO_x composite, as shown in Figure 2(c-f). The XPS spectrum in the C 1s region (Fig. 2c) is quite complex, showing a total of seven components, including peaks assigned to the Ru 3d photoelectrons, at 282.7 eV (Ru 3d5/2) and at 284.6 and 287.5 eV (Ru 3d3/2).[37,39-42] The C 1s peak of the original N-rGO can be deconvoluted into four components. The most intense peak at 284.8 eV is assigned to C=C/C-C, which, together with the component at 289.3 eV that corresponds to C=O/O-C=O, is a signature of graphene obtained via the hydrothermal method. In addition, two peaks at 285.9 and 287.5 eV result from sp2 C-N and sp3 C-N bonding. The same information for nitrogen is shown in Fig. 2(d), where the N peak of the original N-rGO can be deconvoluted into three different components, at 398.3, 400.1, and 401.4 eV, corresponding to pyridinic, pyrrolic, and graphic types of nitrogen, respectively.[43-45] In order to confirm the hydrous nature of the as-synthesized RuO_x nanoparticles in the composite, although ruthenium is typically analyzed by the strong signals from the 3d photoelectrons, here we used the 3p spectrum instead in order to avoid interference from the carbon substrate. The Ru 3p3/2 peak in Fig. 2(e) was deconvoluted into two components, which were identified with RuO (467.1 eV) and RuO_2 (463.8 eV). A signal with a similar ratio is estimated from Ru-O-Ru, identified at 528.9 eV, and Ru-O-H, centred at 530.2 eV (Fig. 2f).[37,39-42]

High ionic conductivity is one of the most important prerequisites of materials for application in electrolyte. The temperature dependent ionic conductivity of the gel-polymer electrolyte with various polymerization times was examined using the AC impedance spectroscopy technique. With extended polymerization time, the ionic conductivity of the electrolyte tends to decrease (Fig. S3). This observation is largely attributed to the formation of a solid structure that restricts the mobility of the lithium ions when compared with the liquid electrolyte. On increasing the testing temperature, the electrolyte ionic conductivity experiences an increasing trend due to the kinetic influence. Meanwhile, it is worth calculating the activation energy (E_a). The activation energy of different gel-polymer electrolytes with various polymerization times was calculated (see SI for details), and the results are shown in Fig. 3(a). GPE with 5 s polymerization time has lower activation energy, 16.1 kJ mol^{-1}, than GPE with 10 s (17.8 kJ mol^{-1}) and 15 s (19.6 kJ mol^{-1}). A low E_a value for a gel electrolyte indicates facile ionic transport along the conducting channels. Therefore, it is reasonable to assume from the above results that the increasing thickness of the solid layer decreases the electrolyte ionic conductivity and increases the activation energy of the electrolyte. In order to test the oxygen permeability of the GPE with different polymerization times, small bottles containing lithium foil and using GPE as the cover were kept in pure oxygen atmosphere. After several days, the lithium metal was still shining when kept under GPE with longer polymerization time (Fig. S4). Therefore, the solid layer can efficiently slow down the oxygen diffusion rate. To investigate the electrochemical stability of the GPE, linear sweep

voltammetry (LSV) measurements were carried out in the potential range between 3.0 and 6.0 V (V vs. Li/Li^+) at a scan rate of 5.0 mV s^{-1}. As shown in Fig. 3(b), no obvious significant oxidation current was observed below 5.0 V, indicating that the obtained gel-polymer electrolyte samples were electrochemically stable up to 5.0 V, so that they could be applied in high voltage batteries. These results were in agreement with previous results. [46]

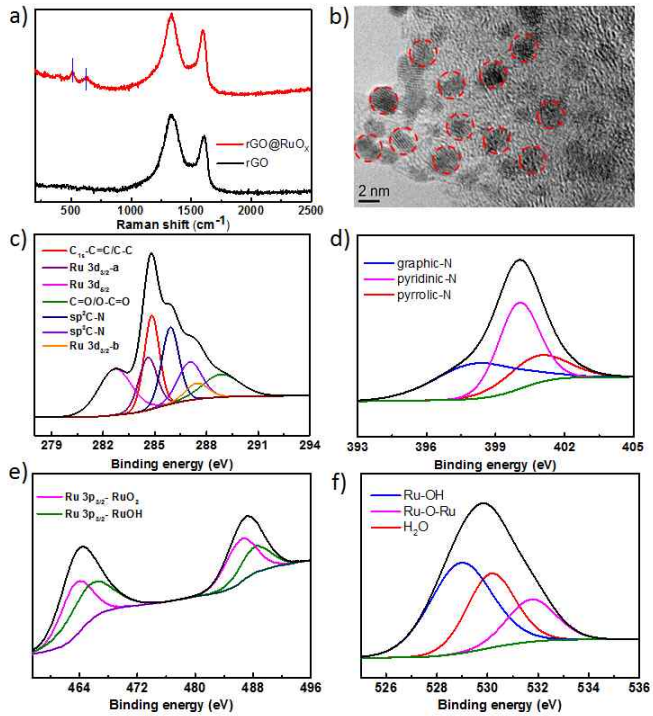

Figure 2. (a) Raman spectra for rGO and N-rGO@RuO_x composite; (b) HRTEM image of the N-rGO@RuO_x composite; XPS results for N-rGO@RuO_x composite: (c) Carbon XPS data; (d) Nitrogen XPS data; (e, f) Ruthenium XPS data.

The electrochemical properties were then examined in pure oxygen atmosphere. The rate performance of the cell using GPE with 5 s polymerization time with a fixed specific capacity of 1000 mAh $g^{-1}_{(composite)}$ is shown in Fig. 3c. At the current densities of 0.1, 0.4, 0.6 and 0.9 mA cm^{-2}, it exhibits lower overpotential and excellent round trip efficiency. At the same time, reversibility of the catalyst is also shown in Fig. 3d. Compared with the pristine electrode, there is clear evidence of crystalline Li_2O_2 formation at the end of discharge. In the following charging, the discharge products become barely visible and cannot be detected, which is consistent with the results obtained by other groups.[5,7,12,14,46] The high catalytic activity of RuO_x together with the high ionic conductivity of the gel-polymer electrolyte plays an important role in the formation and decomposition process.

The GPE-5s sample was compared with normal liquid electrolyte in Fig. 3(e). The cell using liquid electrolyte showed stability during the first 40 cycles, following by a slow decrease until 65 cycles. Then, the cell died, which largely resulted from the drying out of the liquid electrolyte and lithium metal oxidation after long-term cycling, from the evidence cell disassembly in Fig. S5. Compared with liquid electrolyte, the cell using GPE with 5 s polymerization time shows a stable cycling performance, and the voltage obtained at the discharge terminal is higher than 2.2 V for 140 cycles with 0.4 mA cm^{-2} current density. There are also no obvious chemical bonding changes as shown in the FT-IR results (Fig.S6), which indicates the hybrid gel/solid state electrolyte keeps a highly stability during the discharge and charge. In addition, in Fig. 3(f), the device using GPE with 5 s polymerization time also shows a lower overpotential and high round trip efficiency than the normal liquid electrolyte even after the 20th cycle. Meanwhile, the stability of the GPE with 5s polymerization time after cycling was tested using the same technique in Fig. S6, where even after 140 cycles, the gel polymer electrolyte still exhibits high stability when the working potential is lower than V. The excellent cycling performance was largely attributed to the low evaporation rate and higher stability of the GPE-5s electrolyte, as well as the protection of the lithium metal anode during long-term cycling.

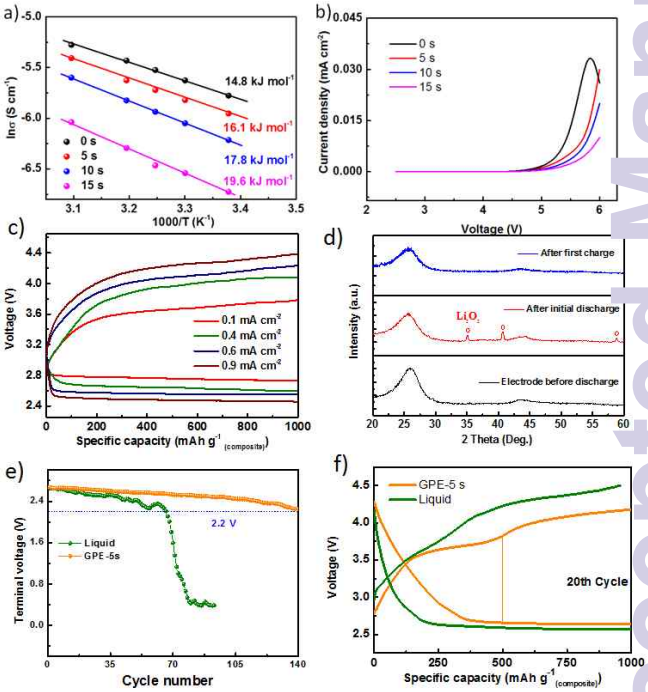

Figure 3. (a) Activation energy of the gel-solid-state polymer electrolyte with different degrees of polymerization; (b) stability of the gel-solid-state polymer electrolyte with different degrees of polymerization; c) First discharge-charge curves of the cell using GPE with 5 s polymerization time at different current densities of 0.1, 0.4, 0.6, and 0.9 mA cm^{-2}, with a capacity of 1000 mAh $g^{-1}_{(composite)}$; d) XRD patterns of the cathode electrode collected at different reaction steps (current density = 0.4 mA cm^{-2}) (e) cycling performance of cell using liquid and GPE-5s electrolyte; (f) Discharge/charge curves for the 20th cycle for cells using liquid and GPE-5s electrolyte.

In addition, for further research on a flexible battery, the battery (inset image in Fig. 4b) was bent and tested in oxygen atmosphere. In Fig. 4, it shows an excellent discharge and charge curve in the first cycle and demonstrates good cycling performance. After 10 cycles, however, the overpotential was greatly increased, and the terminal voltage was also decreased significantly, which may have resulted from the bridge connection resistance due to bending.

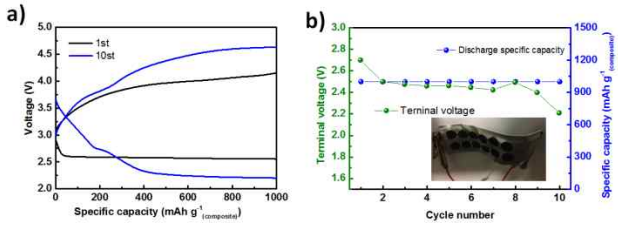

Figure 4. Electrochemical performance of bent lithium oxygen battery: (a) discharge and charge curves of the 1st and 10th cycles; (2) cycling performance of the battery (inset image is photograph of bent battery).

Conclusions

A hybrid gel-solid-state polymer electrolyte has been synthesized and used as the separator and electrolyte for a flexible lithium oxygen battery. Compared with the generally used liquid electrolyte, it shows high ionic conductivity and low activation energy, and it also can not only avoid electrolyte evaporation, but also protects the lithium metal anode during the reactions in long-term cycling. Excellent cycling performance is also demonstrated, in which the terminal voltage is higher than 2.2 V after 140 cycles at 0.4 mA cm^{-2}, with 1000 mAh $g^{-1}_{(composite)}$ limited capacity. Therefore, this gel-solid-state polymer electrolyte is promising for use as a separator as well as an electrolyte for lithium oxygen batteries with good mechanical flexibility in the future.

Acknowledgements

The authors are grateful for funding from Australian Research Council (ARC) through Discovery Project (DP140100401). The authors also thank Dr. T. Silver for critical reading of the manuscript.

Notes and references

[a]Institute for Superconducting and Electronic Materials, University of Wollongong, Wollongong, NSW 2522 Australia
*Email: shulei@uow.edu.au
[b]Department of Energy and Materials Engineering, Dongguk University-Seoul, Seoul, 100-715, Republic of Korea
*Email: dake1234@dongguk.edu
[c]School of Materials and Metallurgy, Northeastern University, Shenyang 110004, China
† Electronic Supplementary Information (ESI) available: [details of experiment details, XRD, FTIR, TEM and conductivity results]. See DOI: 10.1039/c000000x/

1. R. Black, B. Adams and L. F. Nazar, *Adv Energy Mater*, **2012**, 2, 801-815.
2. P. G. Bruce, S. A. Freunberger, L. J. Hardwick and J. M. Tarascon, *Nat Mater*, **2012**, 11, 19.
3. Y. Y. Shao, S. Park, J. Xiao, J. G. Zhang, Y. Wang and J. Liu, *Acs Catal*, **2012**, 2, 844.
4. Y. C. Lu, B. M. Gallant, D. G. Kwabi, J. R. Harding, R. R. Mitchell, M. S. Whittingham and Y. Shao-Horn, *Energ Environ Sci*, **2013**, 6, 750.
5. Z. Q. Peng, S. A. Freunberger, Y. H. Chen and P. G. Bruce, *Science*, **2012**, 337, 563.
6. J. J. Xu, D. Xu, Z. L. Wang, H. G. Wang, L. L. Zhang and X. B. Zhang, *Angew Chem Int Edit*, **2013**, 52, 3887.
7. Z. L. Jian, P. Liu, F. J. Li, P. He, X. W. Guo, M. W. Chen and H. S. Zhou, *Angew Chem Int Edit*, **2014**, 53, 442.
8. B. Sun, X. D. Huang, S. Q. Chen, J. Q. Zhang and G. X. Wang, *Rsc Adv*, **2014**, 4, 11115.
9. S. M. Han, J. H. Kim and D. W. Kim, *J Electrochem Soc*, **2014**, 161, A856.
10. M. D. Bhatt, H. Geaney, M. Nolan and C. O'Dwyer, *Phys Chem Chem Phys*, 2014, 16, 12093.
11. M. Balaish, A. Kraytsberg and Y. Ein-Eli, *Phys Chem Chem Phys*, **2014**, 16, 2801.
12. Y. G. Wang and Y. Y. Xia, *Nat Chem*, **2013**, 5, 445.
13. F. J. Li, T. Zhang, Y. Yamada, A. Yamada and H. S. Zhou, *Adv Energy Mater*, **2013**, 3, 532.
14. K. N. Jung, J. I. Lee, J. H. Jung, K. H. Shin and J. W. Lee, *Chem Commun*, **2014**, 50, 5458.
15. T. Zhang and H. S. Zhou, *Nat Commun*, **2013**, 4.
16. E. Nasybulin, W. Xu, M. H. Engelhard, Z. M. Nie, S. D. Burton, L. Cosimbescu, M. E. Gross and J. G. Zhang, *J Phys Chem C*, **2013**, 117, 2635.
17. O. Borodin, G. D. Smith and W. Henderson, *J Phys Chem B*, **2006**, 110, 1687.
18. I. Stepniak, *J Power Sources*, **2014**, 247, 112.
19. Y. S. Zhu, F. X. Wang, L. L. Liu, S. Y. Xiao, Z. Chang and Y. P. Wu, *Energ Environ Sci*, **2013**, 6, 618
20. A. Hofmann, M. Schulz and T. Hanemann, *Electrochim Acta*, **2013**, 89, 823.
21. M. Ulaganathan, R. Nithya, S. Rajendran and S. Raghu, *Solid State Ionics*, **2012**, 218, 7
22. C. Gerbaldi, J. R. Nair, G. Meligrana, R. Bongiovanni, S. Bodoardo and N. Penazzi, *Electrochim Acta*, **2010**, 55, 1460.
23. X. Wang, Q. Qu, Y. Hou, F. Wang and Y. Wu, *Chem Commun*, **2013**, 49, 6170.
24. Y. Zhu, S. Xiao, Y. Shi, Y. Yang and Y. Wu, J Mater Chem A, **2013**, 1, 7790.
25. Y. Zhu, F. Wang, L. Liu, S. Xiao, Z. Chang and Y. Wu, *Energ Environ Sci*, **2013**, 6, 618.
24. C. Masquelier, *Nat Mater*, **2011**, 10, 648.
25. U. K. Sur, *Curr Sci India*, **2011**, 101, 1129.
26. N. Kamaya, K. Homma, Y. Yamakawa, M. Hirayama, R. Kanno, M. Yonemura, T. Kamiyama, Y. Kato, S. Hama, K. Kawamoto and A. Mitsui, *Nat Mater*, **2011**, 10, 682.
27. J. R. Harding, Y.-C. Lu, Y. Tsukada and Y. Shao-Horn, *Phys Chem Chem Phys*, **2012**, 14, 10540.
28. M. G. Walter, E. L. Warren, J. R. McKone, S. W. Boettcher, Q. Mi, E. A. Santori and N. S. Lewis, *Chem Rev*, **2010**, 110, 6446.
29. Y.-H. Fang and Z.-P. Liu, *J Am Chem Soc*, **2010**, 132, 18214.
30. S. Wendt, A. P. Seitsonen and H. Over, *Catal Today*, **2003**, 85, 167.
31. Y. D. Kim, H. Over, G. Krabbes and G. Ertl, *Top Catal*, **2000**, 14, 95.
32. B. Zhang, C. Zhang, H. He, Y. Yu, L. Wang and J. Zhang, *Chem Mater*, **2010**, 22, 4056.
33. D. R. Rolison, P. L. Hagans, K. E. Swider and J. W. Long, *Langmuir*, **1999**, 15, 774.
34. F. Li, J. Chen, Q. Zhang and Y. Wang, *Green Chem*, **2008**, 10, 553.
35. H. G. Jung, Y. S. Jeong, J. B. Park, Y. K. Sun, B. Scrosati and Y. J. Lee, *Acs Nano*, **2013**, 7, 3532.
36. Y. Lee, J. Suntivich, K. J. May, E. E. Perry and Y. Shao-Horn, *The Journal of Physical Chemistry Letters*, **2012**, 3, 399.
37. W. Wang, S. R. Guo, I. Lee, K. Ahmed, J. B. Zhong, Z. Favors, F. Zaera, M. Ozkan and C. S. Ozkan, *Sci Rep-Uk*, **2014**, 4.
38. H. C. Jo, K. M. Kim, H. Cheong, S.-H. Lee and S. K. Deb, *Electrochemical and Solid-State Letters*, **2005**, 8, E39.
39. K. Vaarmets, S. Sepp, J. Nerut, E. Hark, I. Tallo and E. Lust, *J Solid State Electr*, **2013**, 17, 1729.
40. B. Hudec, K. Husekova, A. Rosova, J. Soltys, R. Rammula, A. Kasikov, T. Uustare, M. Micusik, M. Omastova, J. Aarik and K. Frohlich, *J Phys D Appl Phys*, **2013**, 46.
41. M. F. Lu, X. L. Deng, J. C. Waerenborgh, X. J. Wu and J. Meng, *Dalton T*, **2012**, 41, 11507.
42. S. Bang, S. Lee, T. Park, Y. Ko, S. Shin, S. Y. Yim, H. Seo and H. Jeon, *J Mater Chem*, **2012**, 22, 14141.
43. G. Wu, N. H. Mack, W. Gao, S. G. Ma, R. Q. Zhong, J. T. Han, J. K. Baldwin and P. Zelenay, *Acs Nano*, **2012**, 6, 9764.
44. P. Chen, T. Y. Xiao, H. H. Li, J. J. Yang, Z. Wang, H. B. Yao and S. H. Yu, *Acs Nano*, **2012**, 6, 712.
45. A. Mukherji, B. Seger, G. Q. Lu and L. Z. Wang, *Acs Nano*, **2011**, 5, 3483.
46. S. H. Oh, R. Black, E. Pomerantseva, J. H. Lee and L. F. Nazar, *Nat Chem*, **2012**, 4, 1004.